Journal of Materials Science: Materials in Electronics (2019) 30:14430–14444
https://doi.org/10.1007/s10854-019-01813-z

Structural, magnetic, critical behavior and phenomenological investigation of magnetocaloric properties of $La_{0.6}Ca_{0.4-x}Sr_xMnO_3$ perovskite

M. Jeddi[1] · H. Gharsallah[1,2] · M. Bekri[3] · E. Dhahri[1] · E. K. Hlil[4]

Received: 12 March 2019 / Accepted: 3 July 2019 / Published online: 8 July 2019

Abstract

Structural, magnetic, critical behavior and magnetocaloric properties of $La_{0.6}Ca_{0.4-x}Sr_xMnO_3$ (x = 0.0, 0.1 and 0.4) compounds have been investigated. Rietveld refinement of the X-ray diffraction patterns indicates that our samples are pure single phase adopting the rhombohedral structure (R-3c) for x = 0.0 and the orthorombic structure (Pbnm) for x = 0.1 and 0.4. Temperature dependence of magnetization curves exhibit a second order paramagnetic (PM)/ferromagnetic (FM) phase transition at Curie temperature Tc. The critical behavior has been determined through the isothermal magnetization measurements around the critical temperature Tc by means of various techniques such as modified Arrott plot (MAP), Kouvel-Fisher (KF) method and critical isotherm analysis (CIA). The results are fully satisfactory to the requirements of the Widom scaling relation and the universal scaling hypothesis confirming their accuracy. A phenomenological model is applied to describe the magnetocaloric effect (MCE) behavior of compounds under investigation. At $\mu_0 H = 5T$, the obtained RCP values stand for about 98, 77 and 68% of that observed in pure Gd for x = 0.0, 0.1 and 0.4, respectively, making of these materials considered as promising candidates for magnetic refrigeration applications near room temperature. By analyzing the field dependence of the magnetic entropy change data as well as the relative cooling power, it was possible to evaluate the critical exponent values which were found not only agree with those deduced from (MAP), (KF) and (CIA) methods, but they also obey the scaling theory. Our findings confirm the good correlation between the critical behavior and the MCE properties in manganite systems.

1 Introduction

Magnetic refrigeration (MR), an advanceable cooling power system based on the magnetocaloric effect (MCE), is one of the most impressive techniques that initiated intensive research activity in the recent years owing to its energy-efficient, environment-friendly advantages and economical benefits [1, 2]. This novel invention achievement has attracted the attention of scientific and engineering communities as the most efficient, easily accessible, and highly economical cooling technology compared to the existing vapor compression-expansion refrigeration. The magnetocaloric effect (MCE), firstly discovered by Warburg in 1881 [3], is a common property for all magnetic systems. It manifests as an isothermal magnetic entropy change $\left(\Delta S_M\right)$ or an adiabatic temperature change (δT_{ad}) when the magnetic material is exposed to a varying magnetic field.

Since the beginning, the major challenge of research in this area is focused on identifying materials presenting optimal magnetocaloric properties [4–8] notably at low magnetic fields and near room temperature. Various magnetocaloric materials such as $Gd_5(Ge_{1-x}Si_x)$ [9], $MnAs_{1-x}Sb_x$ [10] and $La(Fe_{1-x}Si_x)_{13}$ [11] have been fully characterized and deeply investigated by several research sections so as to devise the most promoter cooling compound. Currently, much attention has been paid to lanthanum manganites of formula $(La_{1-x}M_x)MnO_3$ (where M is a divalent alkali earth

✉ M. Jeddi
marwajeddi@gmail.com

1 Laboratoire de Physique Appliquée, Faculté des Sciences, Université de Sfax, B. P. 1171, 3000 Sfax, Tunisia

2 Institut Préparatoire aux Études d'Ingénieur de Sfax, Université de Sfax, B. P. 1172, 3018 Sfax, Tunisia

3 Physics Department, Rabigh College of Science and Art, King Abdulaziz University, P.O. Box 344, Rabigh 21911, Saudi Arabia

4 Institut Néel, CNRS Université J. Fourier, B. P. 166, 38042 Grenoble, France

ion) [12–14] not only for its dynamic ability for uses in cooling fields [15–17] but also for its impressive magnetic and electrical properties [18–21]. These materials offer a high degree of chemical flexibility, low cost, easy preparation and more importantly the ability to tailor their magnetic transition temperatures close to room temperature by La-site or Mn-site doping. However, the seeking for new manganite series with perovskite structure and new synthesis routes leading to a stronger magnetocaloric effect is still desired [22–24].

The parent compound, $LaMnO_3$ is a charge-transfer insulator with trivalent manganese ions (Mn^{3+}). The doping of La trivalent element with divalent ions induces the appearance of tetravalent manganese (Mn^{4+}) creating holes in the e_g band. The induced holes allow the charge transfer in the e_g state which is highly hybridized with the oxygen 2p state. Owing to the intra-atomic Hund's rule, the charge transfer leads to a ferromagnetic coupling between Mn^{3+} and Mn^{4+} ions which in turn has a significant effect on the electrical conductivity [25, 26]. These behaviors are usually interpreted with the help of double exchange mechanism which was firstly suggested by Zener [27]. This model has been the most prominent underlying physics that describes the simultaneous occurrence of transition from paramagnetic semiconductor to ferromagnetic metal for most hole-doped manganites. In mixed valence manganese oxides, two types of magnetic transition have been observed: a first order magnetic phase transition and a second order magnetic phase transition. It is worth noting that materials undergoing a second order phase transition exhibit a large magnetocaloric effect which is much more suitable for refrigerators applications [28].

To make these issues clear, it is necessary to study in details the critical exponents at the PM/FM transition region. The exploration of critical phenomena in manganites has drawn a great deal of attention at the beginning of the 90's [29] and still remains one of the actual directions in the condensed state physics.

In earlier theoretical works, the critical behavior related to the PM/FM transition in manganites within the double exchange (DE) model was described in the framework of long range mean field theory [30]. Whereas, some researchers have predicted that the critical exponents are in agreement with a short range exchange interaction model [31, 32]. In the light of the large variation of critical exponents for manganites that almost covers all universality classes and the diversity of experimental tools used for their determination, four kinds of different theoretical models, which are the mean field model ($\beta = 0.5$, $\gamma = 1$), the Tricritical mean field model ($\beta = 0.25$, $\gamma = 1$), the 3D Heisenberg model ($\beta = 0.365$, $\gamma = 1.336$) and the 3D Ising model ($\beta = 0.325$, $\gamma = 1.240$) are investigated in order to discuss the critical properties in manganite systems.

In the present paper, a detailed study of structural, magnetic, critical phenomena and magnetocaloric properties of $La_{0.6}Ca_{0.4-x}Sr_xMnO_3$ (x = 0.0, 0.1 and 0.4) samples is reported. The critical exponents are estimated via the isothermal magnetization measurements around Curie temperature by using various techniques such as modified Arrott plot (MAP), Kouvel-Fisher (KF) method and critical isotherm analysis (CIA). The magnetocaloric properties are determined using a phenomenological model which is applied for the simulation of the temperature dependence of magnetization curve. In order to show the intrinsic relation between the critical phenomena and the magnetocaloric properties, the field dependence of the isothermal entropy change data as well as the relative cooling power are analyzed.

2 Experiment

The $La_{0.6}Ca_{0.4-x}Sr_xMnO_3$ compounds were synthesized using the citric-gel method. The starting precursors: $La(NO_3)6H_2O$, $Ca(NO_3)_24H_2O$, $Mn(NO_3)_26H_2O$ and $Sr(NO_3)_2$ were dissolved in distilled water. In order to obtain a transparent stable solution, the citric acid and the ethylene glycol were added. After pre-annealing the mixture at 80 °C to eliminate water excess, the solution was annealed at 120 °C. The obtained powder was calcined at 700 °C for 12 h. Finally, the powder was pressed into pellets and sintered at 900 °C for 18 h.

Structural characterization and phase identification of the prepared specimens were verified by using the powder X-ray diffraction technique with CuKα radiation ($\lambda = 1.5406$ Å), at room temperature, by a step scanning of 0.015° in the range of $20° \leq 2\theta \leq 80°$. Magnetic measurements were performed by BS1 and BS2 magnetometers developed in Louis Neel Laboratory of Grenoble. The measurements of magnetization versus temperature $M(T)$ were obtained under an applied magnetic field of 0.05 T with a temperature ranging from 5 to 450 K. The isothermal magnetization curves $M(\mu_0 H)$ were measured with dc magnetic fields varying from 0 to 5 T.

3 Results and discussion

3.1 Structural analysis

The X-ray diffraction (XRD) patterns of our synthesized samples are presented in Fig. 1a–c. The structure refinement is performed by Rietveld analysis. Our samples are single phase. The $La_{0.6}Ca_{0.4}MnO_3$ sample crystallizes in the rhombohedral structure with R-3c space group. Whereas, $La_{0.6}Sr_{0.4}MnO_3$ and $La_{0.6}Ca_{0.3}Sr_{0.1}MnO_3$ adopt the orthorhombic structure with Pbnm space group.

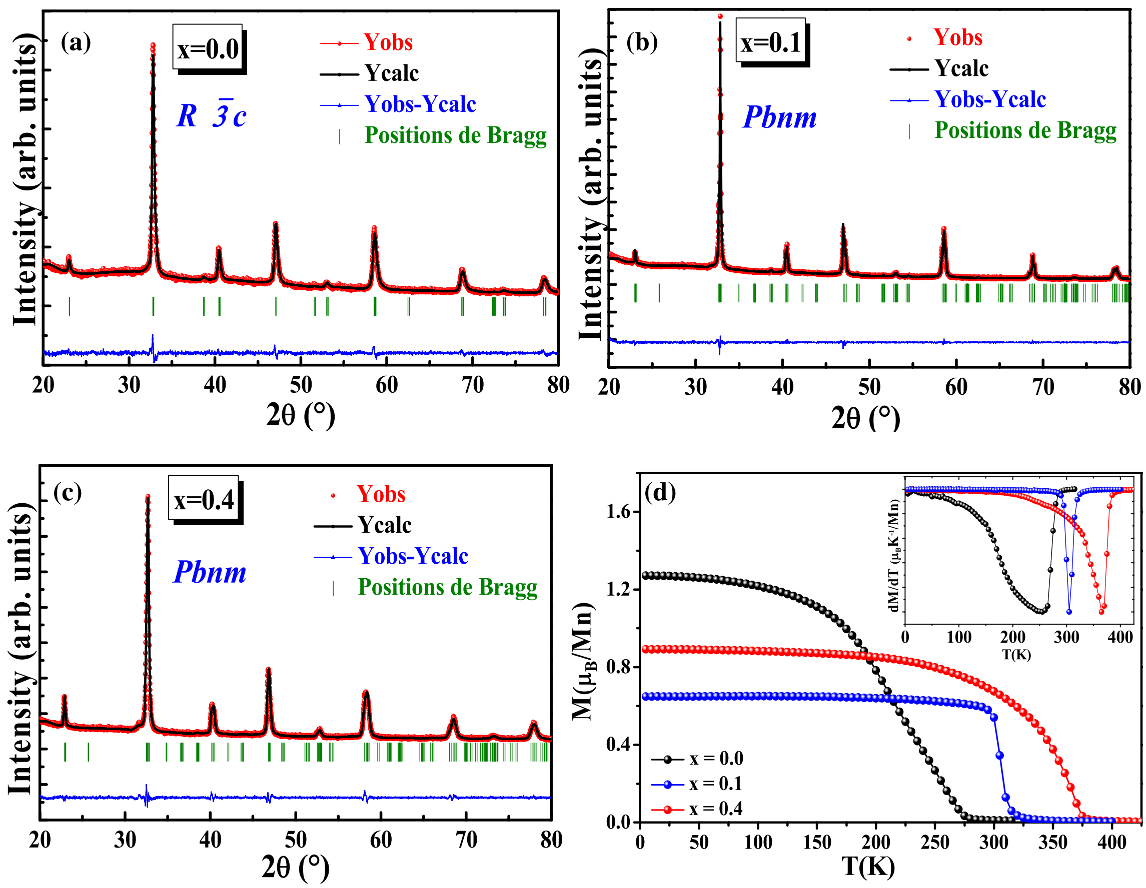

Fig. 1 Powder XRD patterns of $La_{0.6}Ca_{0.4-x}Sr_xMnO_3$ for **a** $x=0.0$, **b** 0.1 and **c** 0.4 compounds. **d** Temperature dependence of magnetization, measured under a magnetic field of 0.05 T, for $La_{0.6}Ca_{0.4-x}Sr_xMnO_3$ ($x=0.0$, 0.1 and 0.4) compounds. The inset presents the dM/dT curves as a function of temperature

Table 1 Results of Rietveld refinement determined from XRD patterns for $La_{0.6}Ca_{0.4-x}Sr_xMnO_3$ for $x=0.0$, 0.1 and 0.4 compounds

Compound	x = 0.0	x = 0.1	x = 0.4
Space group	R$\bar{3}$c	Pbnm	Pbnm
a (Å)	5.457 (1)	5.480 (4)	5.507 (1)
b (Å)	5.457 (1)	5.451 (3)	5.461 (1)
c (Å)	13.371 (2)	7.696 (1)	7.733 (1)
V/FU (Å^3)	57.131	57.477	58.140
$\langle r_A \rangle$(Å)	1.201	1.214	1.253
σ^2 (10^{-4} Å^2)	3.11	12.7	21.20
χ^2(%)	1.733	1.897	1.911

Refinement values of the structural parameters are listed in Table 1. A rapid overview of the obtained structural results shows an increase of the unit cell volume with the increase of Strontium content which is coherent with the increase of the average A-site cationic radius r_A as well as the A-site cation size mismatch σ^2. This increase can be related to the fact that the ionic radius of the Strontium ion ($r(Sr^{2+}) = 1.31$ Å) is larger than that of the Calcium ($r(Ca^{2+}) = 1.18$ Å).

3.2 Magnetic properties

The temperature dependence of magnetization curves carried out under an applied magnetic field of 0.05 T are depicted in Fig. 1d. With decreasing temperature, all compounds exhibit a clear magnetic transition from paramagnetic (PM) to ferromagnetic (FM) state at the Curie temperature Tc, defined as the temperature at which dM/dT shows a minimum (see inset of Fig. 1d). The Curie temperature values are found to be equal to 255 K for $x=0.0$, 304 K for $x=0.1$ and 365 K for $x=0.4$. The increase of Tc should be explained by considering the fact that increasing x increases the average A-site ionic radius r_A (Table 1) which enhances the strength of magnetic exchange interaction between Mn^{3+} and Mn^{4+} and favors the FM order that results in shift of Curie temperature to higher temperature.

The isothermal magnetizations versus the applied magnetic field $M(\mu_0H, T)$ measured at different temperatures are presented in the inset of Fig. 2. Below Tc, the $M(\mu_0 H, T)$ data exhibits a sharp increase at low field region and then a gradual saturation as field value increases reflecting the FM behavior. Above Tc, a drastic decrease of $M(\mu_0 H, T)$ data with an almost linear behavior is noticed indicating the PM behavior.

According to thermodynamics, near the critical point of a second order transition, the free energy G can be expressed in terms of the order parameter M according to the following form:

$$G(T, M) = G_0 + \frac{1}{2}a(T)M^2 + \frac{1}{4}b(T)M^4 - \mu_0 HM, \tag{1}$$

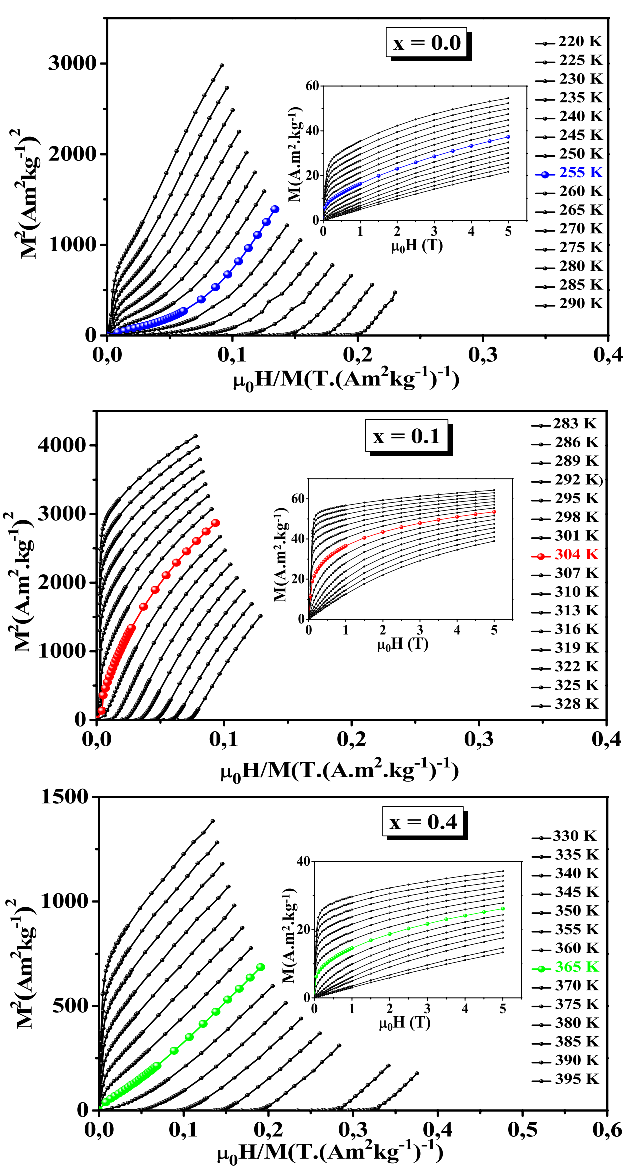

Fig. 2 Arrott plots $(M^2 \text{vs.} \mu_0 H/M)$ measured at different temperatures around Tc for $La_{0.6}Ca_{0.4-x}Sr_xMnO_3$ (x = 0.0, 0.1 and 0.4) compounds. The inset displays the Isothermal magnetization curves

where the coefficients a and b are temperature-dependent parameters.

Using the equilibrium condition at Tc ($\partial G/\partial M = 0$), the obtained relation between the magnetization of the material and the applied field is expressed as follows:

$$\frac{\mu_0 H}{M} = a(T) + b(T)M^2. \tag{2}$$

The main panel of Fig. 2 displays the Arrott plots of $(M^2 \text{vs.} \mu_0 H/M)$ which are constructed from the isothermal magnetization curves. According to Banerjee criterion [33], the order of the magnetic phase transition can be examined through the sign of the slope of Arrott curves $(M^2 \text{vs.} \mu_0 H/M)$. In our case, the slope is positive for all studied temperatures proving that the PM/FM phase transition in the present systems is basically of second order.

3.3 Critical behavior study

According to the scaling hypothesis, a second-order phase transition near the Curie point Tc is characterized by a set of interrelated critical exponents: β (associated with the spontaneous magnetization M_S below Tc), γ (associated with the magnetic susceptibility χ_0^{-1} above Tc) and δ (associated with the critical magnetization isotherm at Tc). Mathematically, these critical exponents are obtained from magnetization measurements through the following asymptotic relations [34]:

$$M_S(T < T_c, \mu_0 H \to 0) = M_0 |\varepsilon|^{\beta}, \tag{3}$$

$$\chi_0^{-1}(T > T_c, \mu_0 H \to 0) = \frac{h_0}{M_0} |\varepsilon|^{\gamma}, \tag{4}$$

$$M(T = T_c, \mu_0 H) = D(\mu_0 H)^{\frac{1}{\delta}}, \tag{5}$$

where $\varepsilon = \frac{T - T_c}{T_c}$ is the reduced temperature and M_0, $\frac{h_0}{M_0}$, and D are the critical amplitudes.

To identify the critical exponents as well as the Curie temperature Tc of our samples, we have used different methods, namely the modified Arrott plots (MAP) method, the Kouvel-Fisher (KF) method and the critical isotherm analysis (CIA).

In the present study, in order to attempt the adequate model leading to a set of reasonably good parallel straight lines and correct exponents, the data was analyzed using a modified Arrott-plot (MAP) expression, based on the Arrott-Noakes equation of state [35]:

$$\left(\frac{\mu_0 H}{M}\right)^{\frac{1}{\gamma}} = a \times \left(\frac{T - T_C}{T}\right) + bM^{\frac{1}{\beta}}, \tag{6}$$

where a and b are considered to be constants.

Figure 3 illustrates the plot of $M^{\frac{1}{\beta}}$ vs. $\left(\frac{\mu_0 H}{M}\right)^{\frac{1}{\gamma}}$ at several temperatures by using different models of critical exponents: the Tri-critical mean field ($\beta = 0.25$, $\gamma = 1$), the 3D Heisenberg model ($\beta = 0.365$, $\gamma = 1.336$) and the 3D Ising model ($\beta = 0.325$, $\gamma = 1.240$). Most models show quasi straight and nearly parallel lines in the high field region. It seems difficult to distinguish which model is the most appropriate to describe our systems.

Here, it is necessary to take into account the so called relative slope (RS) as a new indicator for selection. The RS is defined at the critical point as:

$$RS = \frac{S(T)}{S(T_c)}, \tag{7}$$

where S(T) and S(Tc) are the slopes deduced from (MAP) around and at Tc, respectively.

Figure 4 exhibits the *RS* versus *T* curve of all compounds for the four models: the mean field model, the tri-critical mean field model, the 3D Heisenberg and the 3D Ising. The most satisfactory model should be the one with the closest RS to 1 [36].

It can be observed that the mean field model is the most suitable model to determine the critical behavior of $La_{0.6}Ca_{0.4}MnO_3$ ($x = 0.0$) and $La_{0.6}Sr_{0.4}MnO_3$ ($x = 0.4$) compounds, while the 3D Ising model is the most appropriate model to describe the critical behavior of $La_{0.6}Ca_{0.3}Sr_{0.1}MnO_3$ ($x = 0.1$) compound.

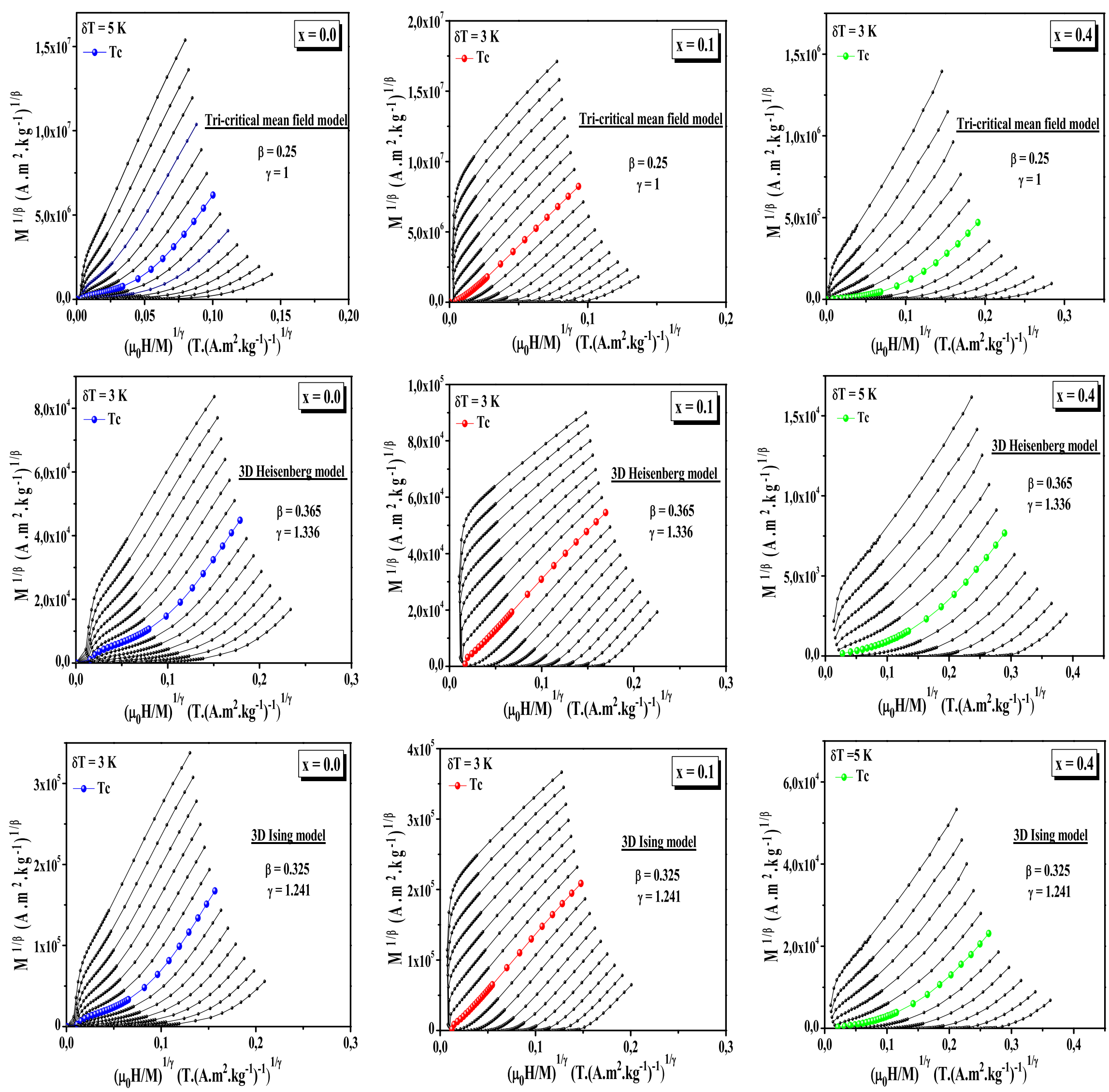

Fig. 3 Modified Arrott plots (MAP): $M^{\frac{1}{\beta}}$ vs. $\left(\mu_0 H/M\right)^{\frac{1}{\gamma}}$ for $La_{0.6}Ca_{0.4-x}Sr_xMnO_3$ for $x = 0.0$, 0.1 and 0.4 compounds, with tri-critical mean field model, 3D Heisenberg model and 3D Ising model

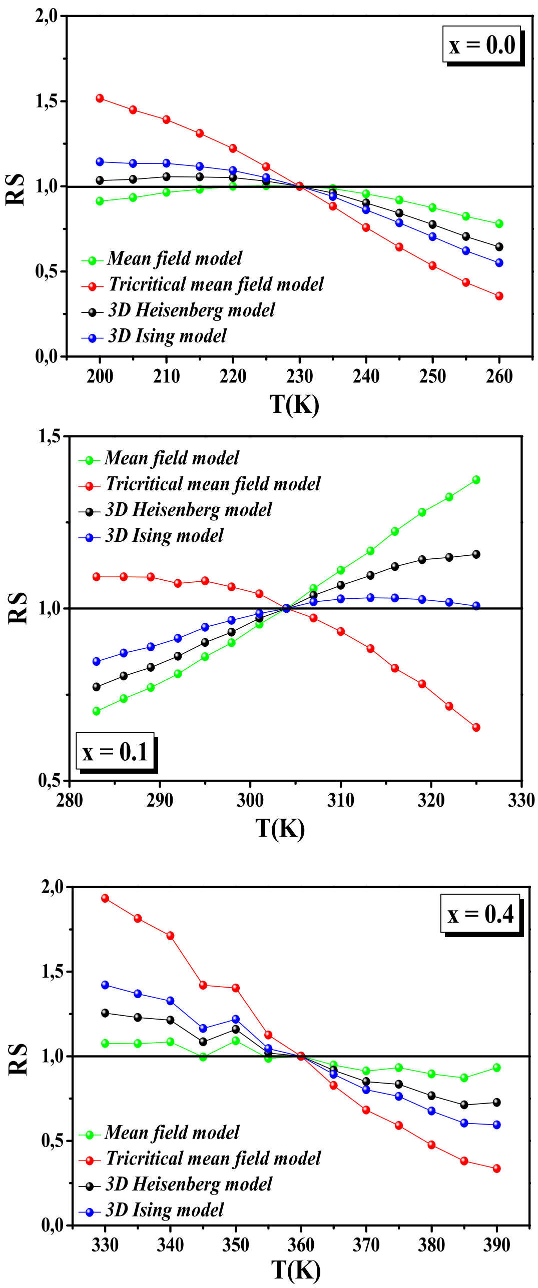

Fig. 4 Relative slope (RS) as a function of temperature for $La_{0.6}Ca_{0.4-x}Sr_xMnO_3$ ($x=0.0$, 0.1 and 0.4) compounds

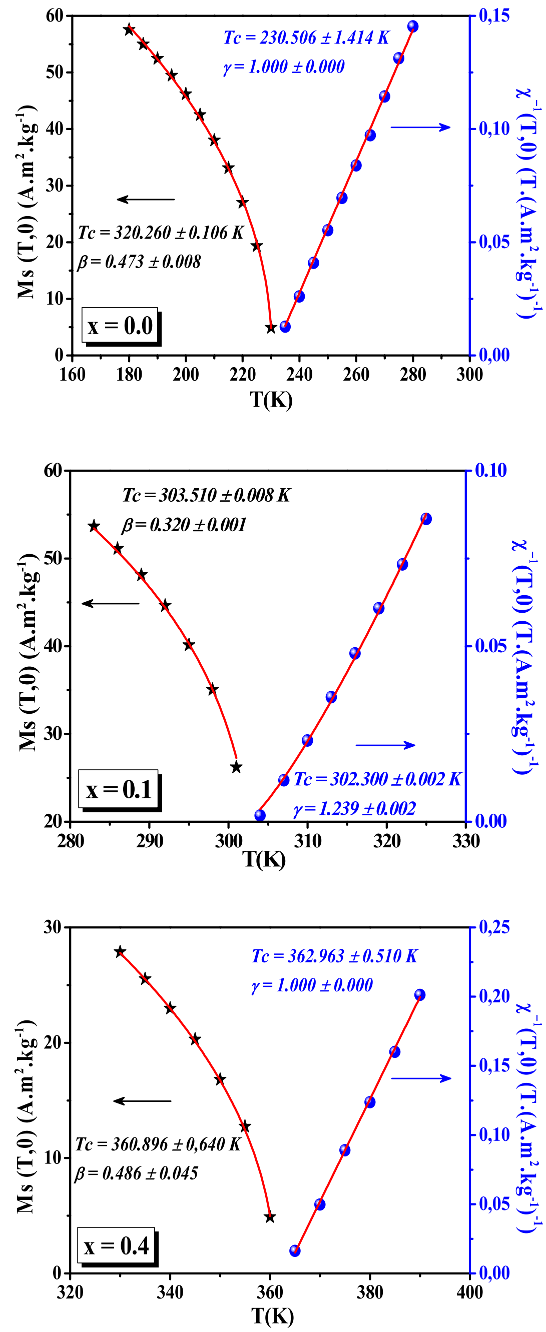

Fig. 5 Temperature dependence of spontaneous magnetization $M_S(T)$ and inverse initial susceptibility $\chi_0^{-1}(T)$ for $La_{0.6}Ca_{0.4-x}Sr_xMnO_3$ ($x=0.0$, 0.1 and 0.4) compounds. The solid lines are the fitting curves of the symbols

According to the (MAP), the linear extrapolation of the high field region of the isotherm provides the values of the spontaneous magnetization M_S and the inverse susceptibility χ_0^{-1} as an intercept on the coordinate axes $M^{\frac{1}{\beta}}$ and $\left(\frac{\mu_0 H}{M}\right)^{\frac{1}{\gamma}}$, respectively. The $M_S(T)$ and $\chi_0^{-1}(T)$ data are reported in Fig. 5. By fitting the $M_S(T)$ and $\chi_0^{-1}(T)$ plots with Eqs. (3) and (4), respectively, new values of β, γ and Tc will be achieved (Table 2).

For more accurate determination of β, γ and Tc values, further processing of $M_S(T)$ and $\chi_0^{-1}(T)$ is performed using the Kouvel-Fisher (KF) method [37] by constructing the functions defined by the following expressions:

$$M_S(T)\left(\frac{dM_S(T)}{dT}\right)^{-1} = \frac{T - T_c}{\beta}, \tag{8}$$

Table 2 Values of the critical exponents of $La_{0.6}Ca_{0.4-x}Sr_xMnO_3$ for $x=0.0$, 0.1 and 0.4 compounds

Model/compound	Technique	Tc (K)	β	γ	δ
Mean field model			0.5	1	3
Tri-critical mean field model			0.25	1	5
3D Heisenberg model			0.365	1.336	4.80
3D Ising model			0.325	1.240	4.82
$La_{0.6}Ca_{0.4}MnO_3$ (x = 0.0)	MAP	230.3 ± 0.1	0.47 ± 0.01	1.00 ± 0.00	
	KF	231.2 ± 0.1	0.47 ± 0.00	1.040 ± 0.007	
	CIA (exp.)				3.00 ± 0.03
	CIA (cal.)				3.17
$La_{0.6}Ca_{0.3}Sr_{0.1}MnO_3$ (x = 0.1)	MAP	303.51 ± 0.008	0.320 ± 0.001	1.239 ± 0.002	
	KF	303.24 ± 0.001	0.321 ± 0.001	1.231 ± 0.004	
	CIA (exp.)				4.80 ± 0.03
	CIA (cal.)				4.83
$La_{0.6}Sr_{0.4}MnO_3$ (x = 0.4)	MAP	360.9 ± 0.6	0.47 ± 0.05	1.00 ± 0.00	
	KF	360.4 ± 0.2	0.47 ± 0.00	0.99 ± 0.01	
	CIA (exp.)				3.23 ± 0.03
	CIA (cal.)				3.13

$$\chi_0^{-1}(T)\left(\frac{d\chi_0^{-1}(T)}{dT}\right)^{-1} = \frac{T-T_c}{\gamma}. \tag{9}$$

Under this method, the $M_S(T)\left(\frac{dM_S(T)}{dT}\right)^{-1}$ and $\chi_0^{-1}(T)\left(\frac{d\chi_0^{-1}(T)}{dT}\right)^{-1}$ plots (Fig. 6) should yield straight lines with slopes $1/\beta$ and $1/\gamma$, respectively. When extrapolated to the ordinate equal to zero, these straight lines should give intercepts on their T axis equal to the Curie temperature. It is noticed that the values of the critical exponents as well as that of Tc, calculated using the (KF) method, are in a good agreement with those using the (MAP) one (Table 2). Therefore, we can come to conclude that the present calculated methods to study the critical properties are both effective and feasible.

Figure 7 presents the critical isotherm $\left(M\text{vs.}\mu_0H\right)$ curves at Tc = 255, 365 and 304 K for x = 0.0, 0.1 and 0.4, respectively, plotted on a log–log scale. Using Eq. (5), the best fits give the value of the third exponent δ. The obtained values are summarized in Table 2. These values are comparable to those obtained theoretically by the Widom scaling law [38]:

$$\delta = 1 + \frac{\gamma}{\beta}. \tag{10}$$

These results ensure the reliability of the obtained β and γ values.

As confirmation, the accuracy of the obtained critical exponent values can be ascertained with the prediction of the scaling theory in the critical region using the equation below:

$$M\left(\mu_0H,\varepsilon\right) = |\varepsilon|^{\beta} f_{\pm}\left(\frac{\mu_0H}{|\varepsilon|^{\beta+\gamma}}\right), \tag{11}$$

where f_+ for T > Tc and f_- for T < Tc are regular analytic functions.

Figure 8 exhibits the $M|\varepsilon|^{-\beta}\text{vs.}\mu_0H|\varepsilon|^{-\beta-\gamma}$ plot using the values of β, γ, and Tc obtained by the (KF) method with the inset plotted on a log–log scale. All experiment data collapses into two independent branches, one for temperatures below Tc and the other for temperatures above Tc. This finding confirms that Eq. (11) is obeyed over the entire range of the normalized variables, which denotes the reliability of the obtained critical exponents and that of Tc.

3.4 Magnetocaloric properties

3.4.1 Theoretical considerations

Based on the phenomenological model, described in Ref. [39], the dependence of magnetization on the variation of temperature and Curie temperature Tc may be written as:

$$M\left(T,\mu_0H\right) = \frac{M_i - M_f}{2}\tanh\left(A\left(T_c - T\right)\right) + BT + C \tag{12}$$

where

- M_i and M_f are respectively the initial and final values of magnetization at FM/PM transition.
- $A = \dfrac{2\left(B - S_c\right)}{M_i - M_f}$
- $B = \left(\frac{dM}{dT}\right)_{T\approx Ti}$ is the magnetization sensitivity (dM/dT) in the ferromagnetic region before transition.

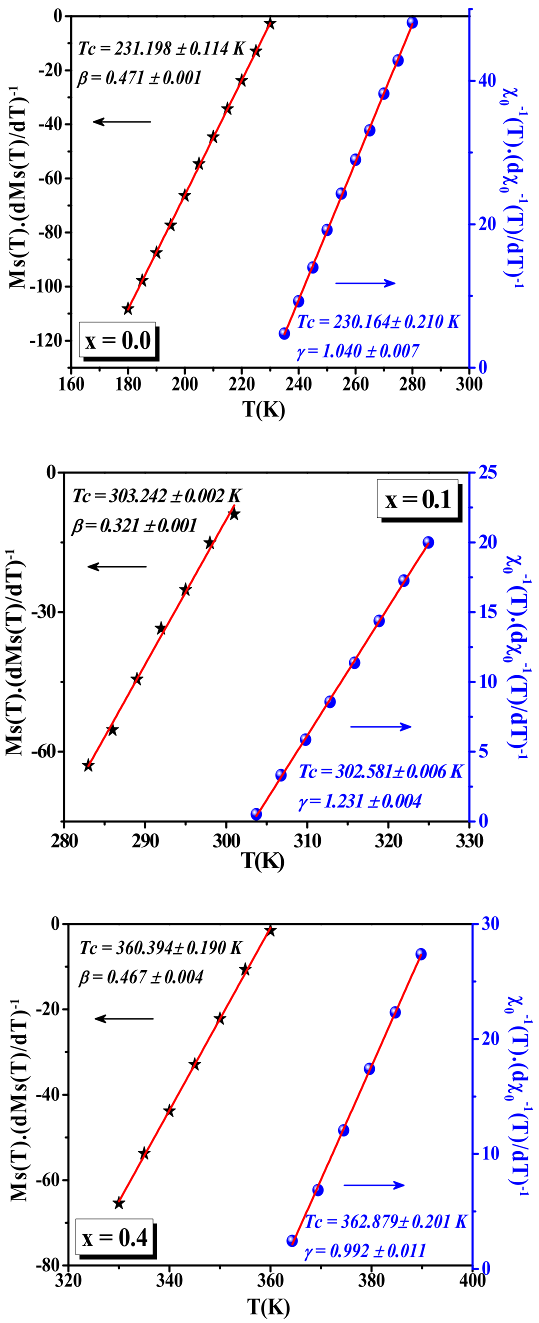

Fig. 6 Kouvel-Fisher (KF) plots for $M_S(T)$ and $\chi_0^{-1}(T)$ for $La_{0.6}Ca_{0.4-x}Sr_xMnO_3$ (x=0.0, 0.1 and 0.4) compounds. The solid lines are the linear fits of the symbols

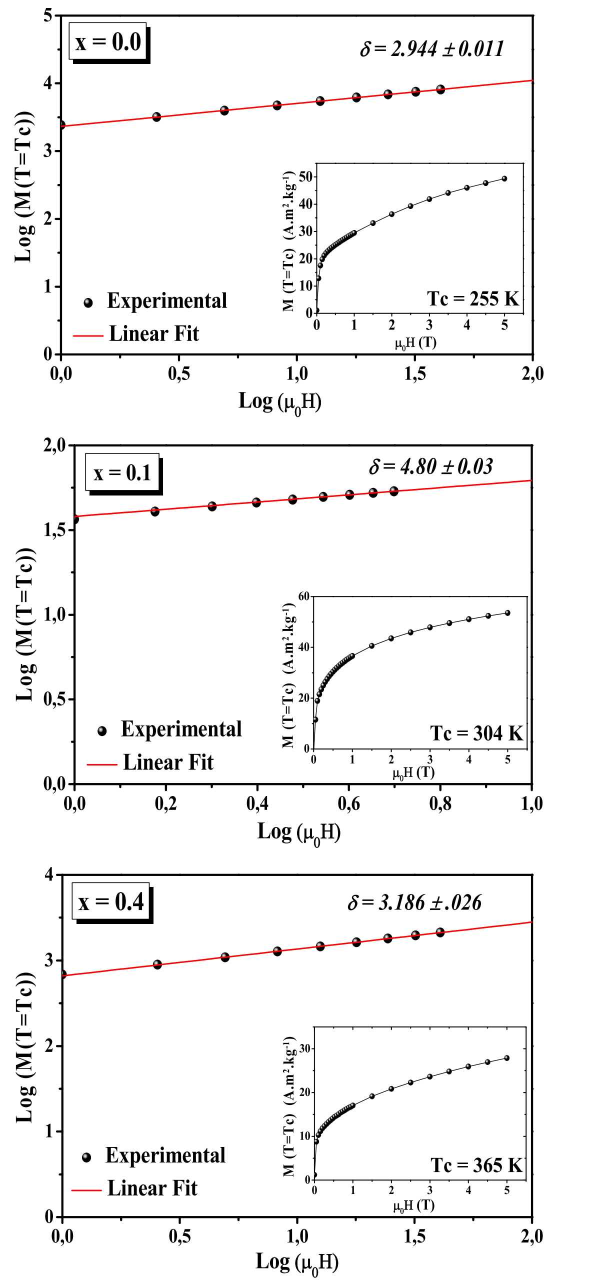

Fig. 7 Critical isotherm $(M\text{vs.}\mu_0 H)$ for $La_{0.6}Ca_{0.4-x}Sr_xMnO_3$ (x=0.0, 0.1 and 0.4) compounds. The inset exhibits the same curve on log–log scale

- $Sc = \left(\frac{dM}{dT}\right)_{T=T_c}$ is the magnetization sensitivity (dM/dT) at Curie temperature Tc.
- $C = \dfrac{M_i + M_f}{2} - BT_c$

The magnetic entropy change (ΔS_M) of a magnetic system under adiabatic magnetic field variation from 0 to final value $\mu_0 H_{\max}$ can be evaluated using the following equation:

$$\Delta S_M = \int_0^{\mu_0 H_{\max}} \left(\frac{\partial M}{\partial T}\right)_{\mu_0 H} d(\mu_0 H), \tag{13}$$

from where:

$$\Delta S_M = \mu_0 H_{\max}\left(-A\frac{M_i - M_f}{2}\sec h^2\big(A(T_c - T)\big) + B\right), \tag{14}$$

with: $\sec h = \frac{1}{\cosh}$.

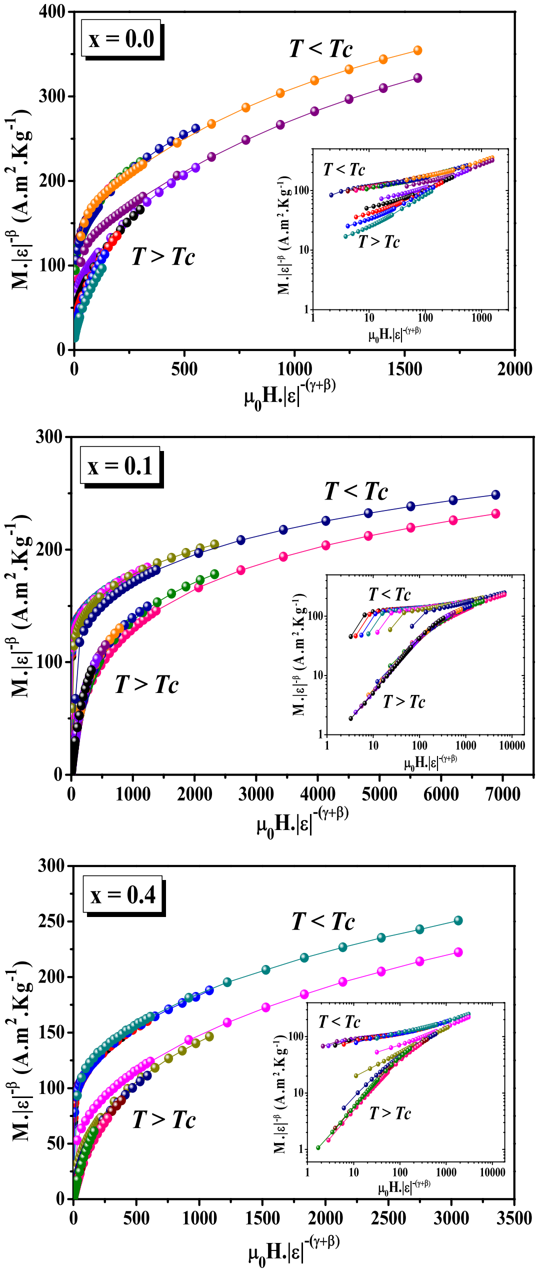

Fig. 8 Scaling plots $M|\varepsilon|^{-\beta}$ vs. $\mu_0 H|\varepsilon|^{-\beta-\gamma}$ below and above Tc for $La_{0.6}Ca_{0.4-x}Sr_xMnO_3$ (x=0.0, 0.1 and 0.4) compounds, The inset exhibits the same curve on log–log scale

The relative cooling power (RCP) is an important parameter to estimate the efficiency of magnetocaloric materials. This latter is defined as the quantity of the heat transfer between the hot and the cold sinks in one ideal refrigeration. It is expressed as:

$$RCP = -\Delta S_M^{\max} \times \delta T_{FWHM}. \tag{15}$$

The maximum entropy change ($\Delta S_M^{\max}$) obtained at T = Tc is given by:

$$\Delta S_M^{\max} = \Delta S_M(T = Tc) = \mu_0 H_{\max}\left(-A\frac{M_i - M_f}{2} + B\right). \tag{16}$$

The full width at half maximum (δT_{FWHM}) is given by:

$$\delta T_{FWHM} = \frac{2}{A}\cosh^{-1}\left(\sqrt{\frac{2A\left(M_i - M_f\right)}{A\left(M_i - M_f\right) + 2B}}\right), \tag{17}$$

from where:

$$RCP = \mu_0 H_{\max}\left(M_i - M_f - 2\frac{B}{A}\right)\cosh^{-1}\left(\sqrt{\frac{2A\left(M_i - M_f\right)}{A\left(M_i - M_f\right) + 2B}}\right). \tag{18}$$

The specific heat change (ΔC_P) can be calculated, from the magnetic contribution to the entropy change induced in the material, by the following expression:

$$\Delta C_P = T\left(\frac{\partial \Delta S_M}{\partial T}\right)_{\mu_0 H} \tag{19}$$

from where:

$$\Delta C_P = TA^2 \mu_0 H_{\max}\left(M_i - M_f\right)\tanh\left(A\left(T_c - T\right)\right)\sec h^2\left(A\left(T_c - T\right)\right) \tag{20}$$

3.5 Model simulation

Figure 9a$_1$–a$_3$ represent the temperature dependence of magnetization curves $M(T)$ for $La_{0.6}Ca_{0.4\text{-}x}Sr_xMnO_3$ (x = 0.0, 0.1 and 0.4) compounds performed under several applied magnetic fields ranging from 1 to 5 T. The $M(T)$ experimental data are fitted using Eq. (12). The symbols display experimental data, while the solid curves exhibit modeled data using fitting parameters listed in Table 3. These parameters were extracted from experimental data. An excellent agreement between both data is noted, indicating the effectiveness of the method adopted for our samples.

With increasing temperature, the $M(T)$ curves exhibit a clear magnetic transition from FM to PM state, without any anomalies detected. We can report that the magnetization displays a continuous change around Curie temperature Tc at different applied magnetic fields indicating the second order of the magnetic phase transition. We can notice a significant decrease of Tc with the decrease of the applied magnetic field.

Figure 9b$_1$–b$_3$ show the predicted results of the magnetic entropy change (ΔS_M) versus temperature at various applied magnetic fields calculated by using Eq. (14). With an increasing of $\left(\mu_0 H\right)$ strength, the peak position of the magnetic entropy change lightly moves to a higher temperature and the magnitude of ΔS_M increases to reach its maximum

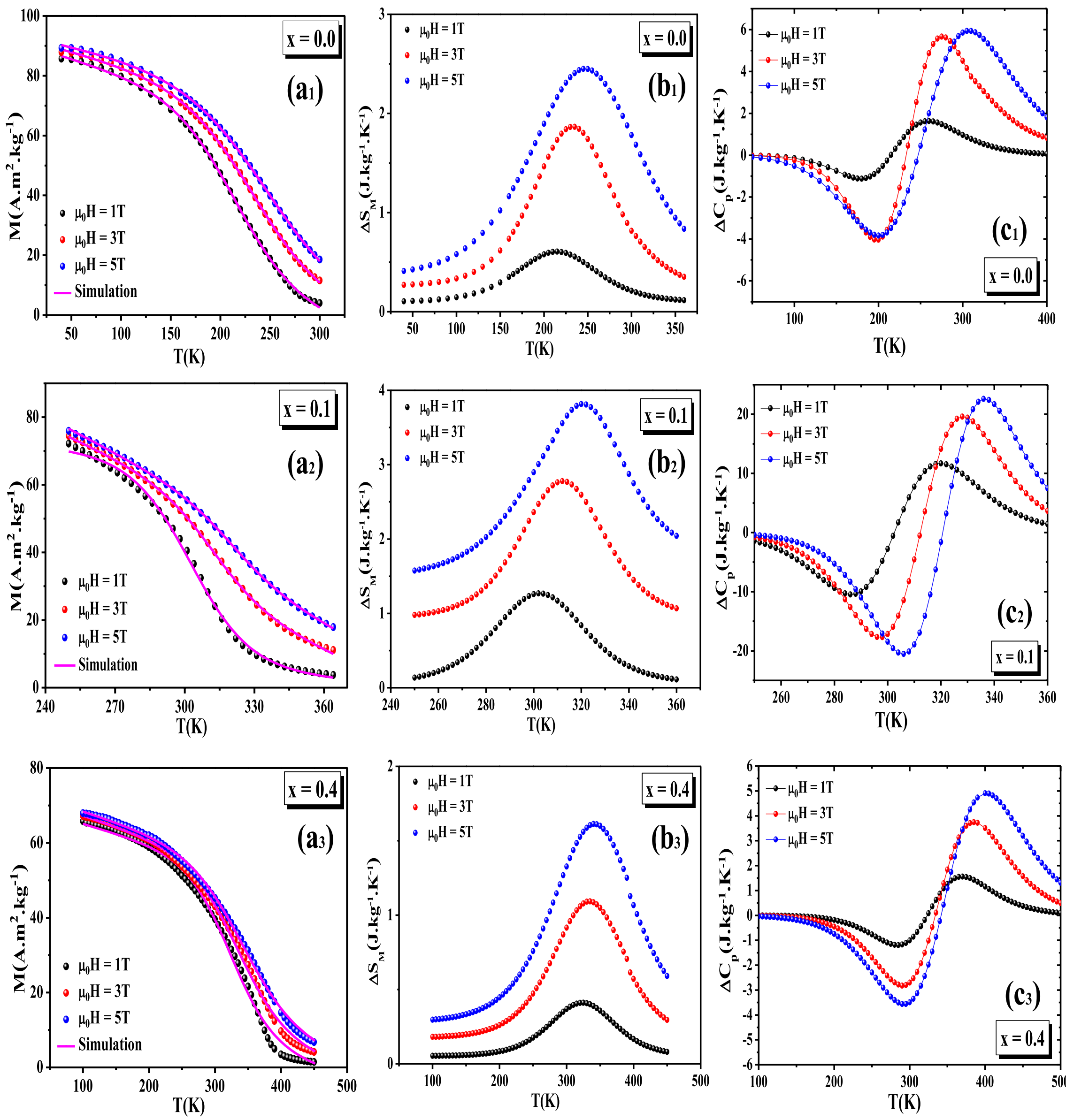

Fig. 9 Temperature dependence of magnetization for $La_{0.6}Ca_{0.4\text{-}x}Sr_xMnO_3$ **a₁** $x=0.0$, **a₂** 0.1 and **a₃** 0.4 compounds at different applied magnetic fields. The solid lines are modeled results and symbols represent experimental data. Magnetic entropy change (ΔS_M) for $La_{0.6}Ca_{0.4\text{-}x}Sr_xMnO_3$ **b₁** $x=0.0$, **b₂** 0.1 and **b₃** 0.4 compounds as a function of temperature at different applied magnetic fields. Specific heat change (ΔC_P) for $La_{0.6}Ca_{0.4\text{-}x}Sr_xMnO_3$ **c₁** $x=0.0$, **c₂** 0.1 and **c₃** 0.4 compounds as a function of temperature at different applied magnetic fields

around Tc. In addition to the magnitude of ΔS_M, the relative cooling power (RCP) defined in Eq. (18) is another important parameter that is used to characterize the refrigerant efficiency of the material. At $\mu_0 H = 5T$, a large value of (RCP) proves to be equal to 400, 314 and 280 J kg^{-1} for $x=0.0$, 0.1 and 0.4, respectively. The obtained (RCP) values stand for about 98, 77 and 68% of that observed in pure Gd [40]. Since the (RCP) factor represents a good way for comparing magnetocaloric materials, our compounds can be considered as an efficient candidates for magnetic refrigeration applications.

Figure 9c_1–c_3 present the predicted results of the specific heat change $\left(\Delta C_P\right)$ versus temperature under different field variations calculated by using Eq. (20). The $\left(\Delta C_P\right)$ undergoes a change from negative to positive around Tc with a negative value below Tc and a positive one above Tc. The negative or positive values of $\left(\Delta C_P\right)$ closely below or above Tc can strongly modify the total specific heat which affects

Table 3 Model parameters for $La_{0.6}Ca_{0.4-x}Sr_xMnO_3$ compounds (x = 0.0, 0.1 and 0.4) at different applied magnetic fields

Materials	$\mu_0 H$ (T)	Tc (K)	M_i (A m^2 kg^{-1})	M_f (A m^2 kg^{-1})	B (A m^2 kg^{-1} K^{-1})	Sc (A m^2 kg^{-1} K^{-1})
$La_{0.6}Ca_{0.4}MnO_3$ (x = 0.0)	1	214.711	73.278	10,652	−0.097	−0.553
	3	232.853	80.000	15.975	−0.086	−0.505
	5	247.082	85.318	16.030	−0.071	−0.218
$La_{0.6}Ca_{0.3}Sr_{0.1}MnO_3$ (x = 0.1)	1	302.501	58.616	6.866	−0.359	−1.341
	3	312.257	62.813	19.040	−0.323	−0.811
	5	320.662	65.584	28.548	−0.303	−0.624
$La_{0.6}Sr_{0.4}MnO_3$ (x = 0.4)	1	323.461	51.731	4.865	−0.051	−0.481
	3	334.071	52.208	8.030	−0.058	−0.412
	5	341.772	54.650	10.250	−0.056	−0.348

the cooling or heating power of the magnetic refrigerator [36].

The values of $\left(-\Delta S_M^{\max}\right)$, $\left(\delta T_{FWHM}\right)$, (RCP) and ($\Delta C_p^{\max}$ and ΔC_p^{min}), calculated in the present study using the relations (16), (17), (18) and (20), respectively, are compared with other magnetic materials at different magnetic fields [40–44] and included in Table 4.

3.6 Phenomenological universal curve

To unveil the nature of the magnetic phase transition in samples, Bonilla et al. [45] have proposed a phenomenological universal curve. The construction of the phenomenological universal curve is based on the collapse of all $\Delta S_M\left(T, \mu_0 H\right)$ data measured at different $\left(\mu_0 H\right)$ into one single new curve in the case of a second order phase transition. This procedure was performed by normalizing the magnetic entropy change curves $\left(\Delta S_M\right)$ with respect to their peak $\left(\Delta S_M^{\max}\right)$ and imposing a scaling law for the temperature axis. The axis of the temperature was rescaled differently below and above Tc, just requiring that the position of the two reference points of each curve corresponds to θ = ± 1:

$$\theta = \begin{cases} -\left(T - T_C\right)/\left(T_{r1} - T_C\right); T \le T_C \\ \left(T - T_C\right)/\left(T_{r2} - T_C\right); T > T_C \end{cases}, \tag{21}$$

where θ is the rescaled temperature, T_{r1} and T_{r2} are the temperature values of the two reference points of each curve. For the present study, T_{r1} and T_{r2} have been selected as those corresponding to $\Delta S_M\left(T_{r1,2}\right) = (1/2)\Delta S_M^{\max}$.

Table 4 The predicted values of magnetocaloric properties for $La_{0.6}Ca_{0.4-x}Sr_xMnO_3$ compounds (x = 0.0, 0.1 and 0.4) compared to other magnetic materials at different applied magnetic fields

Materials	$\mu_0 H$(T)	$-\Delta S_M^{\max}$ (J kg^{-1} K^{-1})	δT_{FWHM} (K)	RCP (J kg^{-1})	$\Delta C_p^{\max}$ (J kg^{-1} K^{-1})	$\Delta C_p^{\min}$ (J kg^{-1} K^{-1})	Refs.
$La_{0.6}Ca_{0.4}MnO_3$ (x = 0.0)	1	0.61	126.36	76.56	1.67	−1.13	Present work
	3	1.61	145.23	234.75	5.64	−4.07	
	5	2.45	166.50	400.01	5.99	−3.82	
$La_{0.6}Ca_{0.3}Sr_{0.1}MnO_3$ (x = 0.1)	1	1.27	46.66	59.20	11.70	−10.47	
	3	2.78	63.05	175.15	19.60	−17.69	
	5	3.81	82.42	314.35	22.58	−20.53	
$La_{0.6}Sr_{0.4}MnO_3$ (x = 0.4)	1	0.41	128.88	52.91	1.63	−1.22	
	3	1.09	148.01	161.69	3.70	−2.83	
	5	1.61	173.33	279.52	4.88	−3.58	
Gd	2	5.5		164			[41]
	5	10.2		410			[40]
$La_{0.75}Sr_{0.1}Ca_{0.15}MnO_3$	2	2.495	31.29	78.083	26.84	−24.24	[42]
	5	5.8	33.65	195.207	28.98	−24.18	
$La_{0.7}(Ba, Sr)_{0.3}MnO_3$	2	1.6	73.56	110.34	4.2	−3.53	[43]
	5	2.75	103.8	285.8	7.44	−6.32	
$La_{0.75}Ca_{0.25}MnO_3$	2	3.75	22.98	86.12	62.34	−58.40	[44]
	4	5.39	33.97	183.16	58.11	−53.19	

The normalized entropy change $\left(\Delta S_M/\Delta S_M^{\max}\right)$ as a function of the rescaled temperature (θ) for all compounds is introduced in Fig. 10. It is clear that all normalized entropy change curves collapse into a single curve reinforcing the second order nature of the FM/PM phase transition observed in our samples [46].

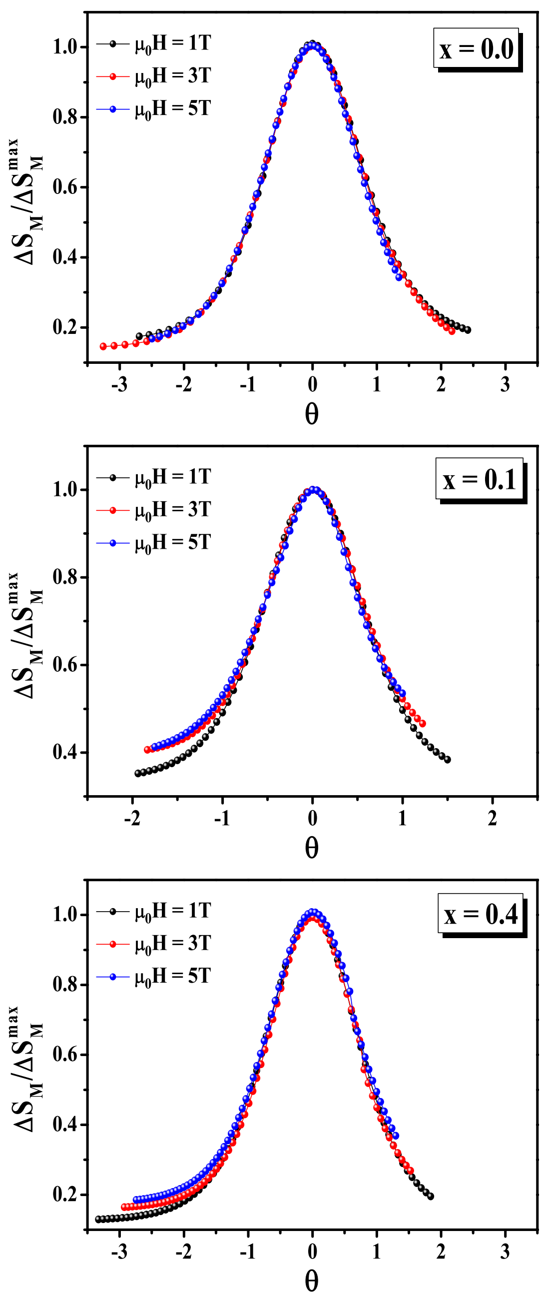

Fig. 10 The master curve behavior of the magnetic entropy change of $La_{0.6}Ca_{0.4-x}Sr_xMnO_3$ (x=0.0, 0.1 and 0.4) compounds as a function of the rescaled temperature

3.7 Correlation between critical exponents and magnetocaloric effect

The field dependence of the magnetic entropy change of second order phase transition magnetic materials can be approximated by a universal law of the field [47]:

$$\Delta S_M \propto \left(\mu_0 H\right)^n \tag{22}$$

where n is assigned to a parameter characteristic of magnetic ordering [47, 48].

The field dependence of the magnetic entropy change of materials under investigation is presented in Fig. 11. By fitting the $\left(\Delta S_M \text{vs.} \mu_0 H\right)$ data, the obtained values of the exponent n are 0.66, 0.56 and 0.71 for x = 0.0, 0.1 and 0.4, respectively.

The field dependence of RCP is also analyzed. It can be expressed as a power law [49]:

$$RCP \propto \left(\mu_0 H\right)^{1+\frac{1}{\delta}}, \tag{23}$$

where δ is the critical exponent of the magnetic transition.

The field dependence of the RCP is presented in Fig. 11. The value of δ deduced from the fitting of $\left(RCP \text{vs.} \mu_0 H\right)$. plot corresponds to 2.51, 4.98 and 2.99 for x = 0.0, 0.1 and 0.4, respectively.

In the particular case of T = Tc, a relationship between the exponent n and the critical exponents β and γ is established as follows [50]:

$$n\left(T_C\right) = 1 + \frac{\beta - 1}{\beta + \gamma}. \tag{24}$$

Since $\beta\delta = \beta + \gamma$ [51], Eq. (24) can be rewritten as:

$$n\left(T_C\right) = 1 + \frac{1}{\delta}\left(1 - \frac{1}{\beta}\right). \tag{25}$$

By associating the value of n and δ following to Eqs. (24) and (25), the obtained values of the critical exponents (β and γ) are (0.54 and 0.82) for x = 0.0, (0.317 and 1.235) for x = 0.1 and (0.53 and 1.06) for x = 0.4. It is worth noting that the values of the critical exponents extracted from the field dependence of the magnetic entropy change perfectly agree with those corresponding to the mean field model (β = 0.5, γ = 1, δ = 3) for $La_{0.6}Ca_{0.4}MnO_3$ and $La_{0.6}Sr_{0.4}MnO_3$ and to the 3D Ising class (β = 0.325, γ = 1.241, δ = 4.82) for $La_{0.6}Ca_{0.3}Sr_{0.1}MnO_3$.

The critical exponents deduced from the field dependence of $\left(\Delta S_M\right)$ and RCP are evidently comparable to those determined by the (KF) method. This result confirms that the critical behavior is well correlated with the MCE properties.

To check the accuracy of the deduced exponents, Franco et al. [52] attempts to scale $\left(\Delta S_M\right)$ in the critical region as follows:

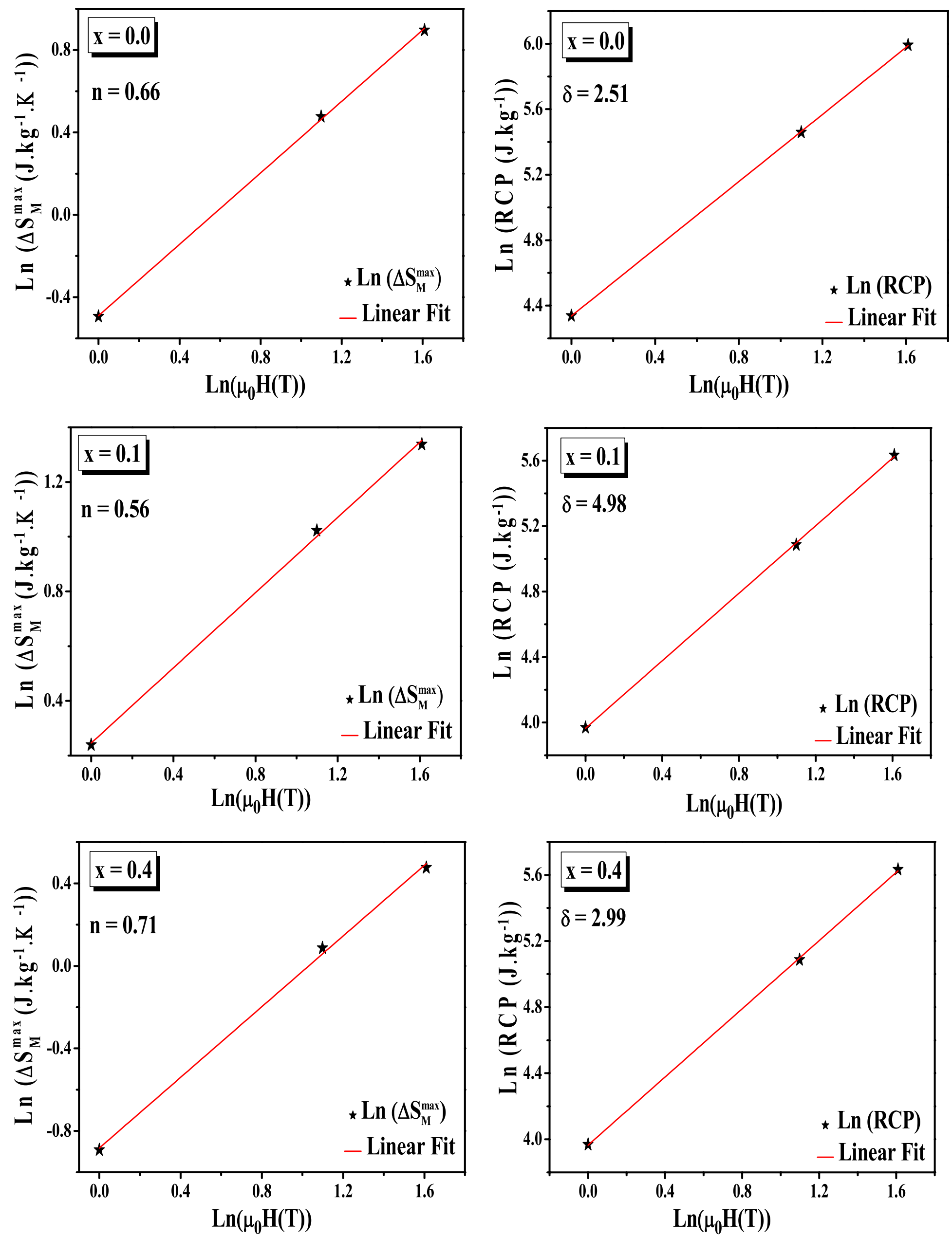

Fig. 11 Variation of $\left(Ln\left(\Delta S_M^{max}\right)$ vs. $Ln\left(\mu_0 H\right)\right)$ and $\left(Ln(RCP)\right.$ vs. $\left.Ln\left(\mu_0 H\right)\right)$ for $La_{0.6}Ca_{0.4-x}Sr_xMnO_3$ ($x = 0.0$, 0.1 and 0.4) compounds

$$-\Delta S_M\left(\mu_0 H, T\right) = \left(\mu_0 H\right)^{\frac{1-\alpha}{\Delta}} f\left(\frac{\varepsilon}{\left(\mu_0 H\right)^{\frac{1}{\Delta}}}\right), \tag{26}$$

where $\alpha = 2 - 2\beta - \gamma$ and $\Delta = \beta + \gamma$ are the usual critical exponents [53] and $\varepsilon = \frac{T_c - T}{T_c}$ is the reduced temperature.

Referring to Eq. (26) and using the appropriate values for the critical exponents, the plot of $\left(\frac{-\Delta S_M(\mu_0 H, T)}{(\mu_0 H)^{\frac{1-\alpha}{\Delta}}}\right)$ vs. $\frac{\varepsilon}{(\mu_0 H)^{\frac{1}{\Delta}}}$ is depicted in Fig. 12 for all compounds. All the experimental data clearly collapse on a single master curve for all measured fields and temperatures indicating the satisfaction of the obtained critical exponent values for these specimens to the requirements of the scaling hypothesis, which further proves their accuracy.

4 Conclusion

To sum up, a descriptive report on structural, magnetic, critical behavior and magnetocaloric properties of $La_{0.6}Ca_{0.4\text{-}x}Sr_xMnO_3$ (x = 0.0, 0.1 and 0.4) samples has been presented. The Rietveld refinement of XRD pattern reveals that sample with x = 0.0 is indexed in the rhombohedral

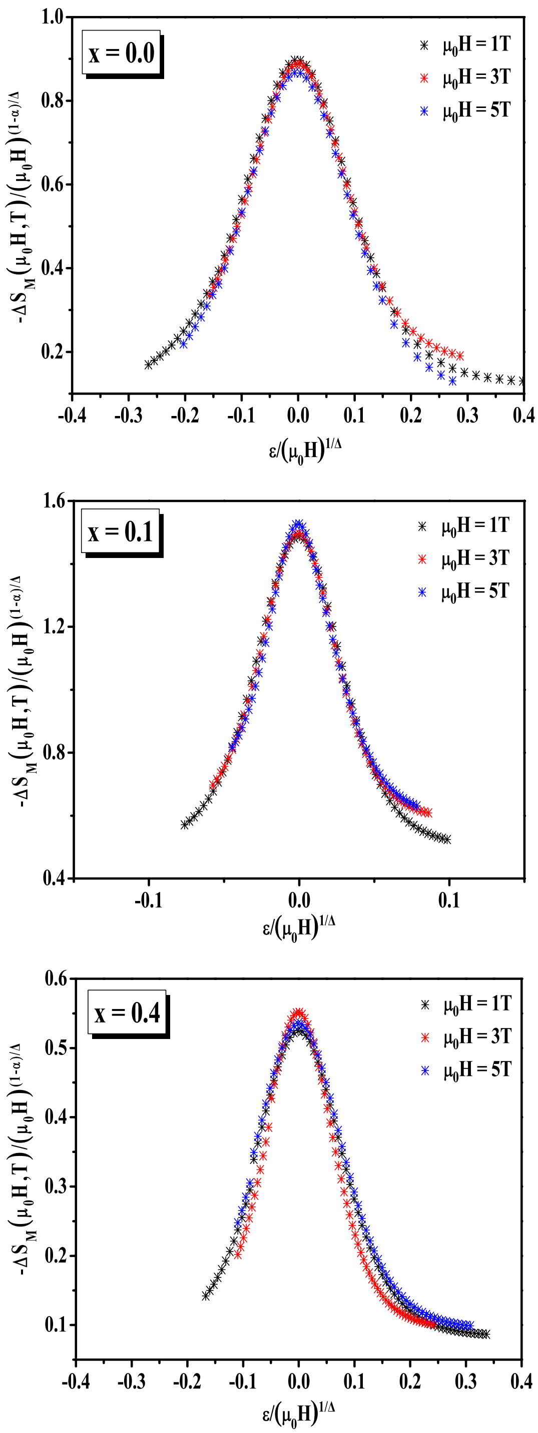

Fig. 12 Scaled magnetic entropy change versus scaled temperature using critical exponents for $La_{0.6}Ca_{0.4-x}Sr_xMnO_3$ (x=0.0, 0.1 and 0.4) compounds

structure (R-3c) whereas those with x = 0.1 and 0.4 are indexed in the orthorombic structure (Pbnm). Magnetic measurements display a second order paramagnetic (PM)/ferromagnetic (FM) phase transition at Curie temperature. By analyzing the isothermal magnetization around the Curie temperature Tc and using various techniques such as modified Arrott plot (MAP), Kouvel-Fisher (KF) method and critical isotherm analysis (CIA), the values of β, γ, δ and Tc are estimated. The validity of the critical exponents is confirmed by the scaling analysis. The second order FM/PM phase transition of $La_{0.6}Ca_{0.4-x}Sr_xMnO_3$ compounds upon different magnetic fields was modeled. Based on this phenomenological model and using thermodynamic calculation, the magnetocaloric properties such as the maximum of the magnetic entropy change $\left(-\Delta S_M^{max}\right)$, the full-width at half-maximum $\left(\delta T_{FWHM}\right)$, the relative cooling power (RCP) and the specific heat change (ΔC_P) were predicted. Significant values of the MCE properties around room temperature are noted. The second order magnetic phase transition already indicated by Banerjee criterion is confirmed by a phenomenological universal curve of the magnetic entropy change. The obtained values of the exponents β, γ and δ extracted from the MCE analysis, are found to obey the scaling theory. These findings prove the intrinsic relation between MCE properties and the universality class.

References

1. E. Bruck, J. Phys. D **38**, R381 (2005)
2. A.M. Tishin, Y.I. Spichin, *The Magnetocaloric Effect and its Applications* (IOP Publishing, London, 2003)
3. E. Warburg, Ann. Phys. **13**, 141 (1881)
4. Y. Yi, L. Li, K. Su, Y. Qi, D. Huo, Intermetallics **80**, 22 (2017)
5. Y. Yang, Y. Zhang, X. Xu, S. Geng, L. Hou, X. Li, Z. Ren, G. Wilde, J. Alloys. Compd. **692**, 665 (2017)
6. Y. Zhang, L. Hou, Z. Ren, X. Li, G. Wilde, J. Alloys. Compd. **656**, 635 (2016)
7. R. Moubah, A. Boutahar, H. Lassri, A. Dinia, S. Colis, B. Hjörvarsson, P.E. Jönsson, Mater. Lett. **175**, 5 (2016)
8. G. Alouhmy, R. Moubah, E.H. Sayouty, H. Lassri, Solid State Commun. **250**, 14 (2017)
9. V.K. Pecharsky, K.A. Gschneidner, J. Phys. Rev. Lett. **78**, 4494 (1997)
10. H. Wada, Y. Tanabe, Appl. Phys. Lett. **79**, 3302 (2001)
11. A. Fujita, K. Fukamichi, IEEE Trans. Magn. **35**, 1796 (1999)
12. M.H. Phan, S.C. Yu, J. Magn. Magn. Mater. **308**, 325 (2007)
13. M. Smari, I. Walha, E. Dhahri, E.K. Hlil, J. Alloys Compd. **579**, 564 (2013)
14. N. Dhahri, A. Dhahri, K. Cherif, J. Dhahri, K. Taibi, E. Dhahri, J. Alloys Compd. **496**, 69 (2010)
15. A. Dhahri, M. Jemmali, E. Dhahri, M.A. Valente, J. Alloys. Compd. **638**, 221 (2015)
16. M. Khlifi, M. Bejar, E. Dhahri, P. Lachkar, E.K. Hlil, J. Appl. Phys. **111**, 103909 (2012)
17. P.K. Siwatch, H. Siugh, O.N. Srivastava, J. Phys.: Condens. Matter **20**, 273201 (2008)
18. Y. Tokura, Rep. Prog. Phys. **69**, 797 (2006)
19. M. Wali, R. Skini, M. Khlifi, M. Bekri, E. Dhahri, E.K. Hlil, Ceram. Int. **42**, 5699 (2016)
20. A. Tozri, E. Dhahri, E.K. Hlil, Mater. Lett. **64**, 2138 (2010)
21. M. Khlifi, A. Tozri, M. Bejar, E. Dhahri, E.K. Hlil, J. Magn. Magn. Mater. **324**, 2142 (2012)
22. M.B. Salamon, M. Jaime, Rev. Mod. Phys. **73**, 583 (2001)

23. H. Baaziz, A. Tozri, E. Dhahri, E.K. Hlil, Chem. Phys. Lett. **625**, 168 (2015)
24. S.B. Tian, M.H. Phan, S.C. Yu, N.H. Hur, Phys. B **327**, 221 (2003)
25. L. Joshi, S. Keshri, Measurement **44**, 938 (2011)
26. S.S. Ata-Allah, M.F. Mostafa, Z. Heiba, H.S. Refai, Physics B **406**, 801 (2011)
27. C. Zener, Phys. Rev. **81**, 440 (1951)
28. V. Franco, A. Conde, Int. J. Refrig **33**, 465 (2010)
29. R.H. Heffner, L.P. Le, M.F. Hundley, J.J. Neumeier, G.M. Luke, K. Kojima, B. Nachumi, Y.J. Uemura, D.E. MacLaughlin, S.W. Cheong, Phys. Rev. Lett. **77**, 1869 (1996)
30. H.E. Stanley, *Introduction to phase Transitions and Critical Phenomena* (Oxford University Press, London, 1971)
31. J.L. Alonso, L.A. Fernandez, F. Guinea, V. Laliena, V. Martin-Mayor, Nucl. Phys. B **596**, 587 (2001)
32. A.K. Pramanik, A. Banerjee, Phys. Rev. B **79**, 214426 (2009)
33. S.K. Banerjee, Phys. Lett. **12**, 16 (1964)
34. K. Huang, *Statistical Mechanics* (Wiley, New York, 1987)
35. A. Arrott, J.E. Noakes, Phys. Rev. Lett. **19**, 786 (1967)
36. A. Schwartz, M. Scheffler, S.M. Anlage, Phys. Rev. B **61**, R870 (2000)
37. J.S. Kouvel, M.E. Fisher, Phys. Rev. B **136**, A1626 (1964)
38. B. Widom, J. Chem. Phys. **43**, 3898 (1965)
39. M.A. Hamad, Phase Trans. **85**, 106 (2012)
40. K.A. Gschneidner Jr., V.K. Pecharsky, A.O. Tsokol, Rep. Prog. Phys. **68**, 1479 (2005)
41. SYu. Dankov, A.M. Tishin, V.K. Pecharsky, K.A. Gschneidner Jr., Phys. Rev. B **57**, 3478 (1998)
42. A. Dhahri, M. Jemmali, E. Dhahri, M.A. Valente, J. Alloys Compd. **638**, 221 (2015)
43. R. Tlili, A. Omri, M. Bejar, E. Dhahri, E.K. Hlil, Ceram. Int. **41**, 10654 (2015)
44. M.A. Hamad, J. Adv. Ceram. **1**, 290 (2012)
45. C.M. Bonilla, J.H. Albillos, F. Bartolomé, L.M. García, M.P. Borderías, V. Franco, Phys. Rev. B **81**, 224424 (2010)
46. J. Fan, W. Zhang, X. Zhang, L. Zhang, Y. Zhang, Mater. Chem. Phys. **144**, 206 (2014)
47. H. Oesterreicher, F.T. Paker, J. Appl. Phys. **55**, 4334 (1984)
48. V. Franco, J.S. Blázquez, A. Conde, Appl. Phys. Lett. **89**, 222512 (2006)
49. A. Dhahri, E. Dhahri, E.K. Hlil, Appl. Phys. A **116**, 2077 (2014)
50. V. Franco, A. Conde, M.D. Kuzmin, J.M. Romero-Enrique, J. Appl. Phys. **105**, 917 (2009)
51. B. Widom, J. Chem. Phys. **43**, 3898 (1965)
52. V. Franco, A. Conde, Int. J. Refrig **33**, 465 (2010)
53. A. Hankey, H.E. Stanley, Phys. Rev. B **6**, 3515 (1972)